

# The hydrogen atom in an electric field: Closed-orbit theory with bifurcating orbits

T Bartsch, J Main and G Wunner

Institut für Theoretische Physik 1, Universität Stuttgart, 70550 Stuttgart, Germany

E-mail: bartsch@theo1.physik.uni-stuttgart.de

**Abstract.** Closed-orbit theory provides a general approach to the semiclassical description of photo-absorption spectra of arbitrary atoms in external fields, the simplest of which is the hydrogen atom in an electric field. Yet, despite its apparent simplicity, a semiclassical quantization of this system by means of closed-orbit theory has not been achieved so far. It is the aim of this paper to close that gap. We first present a detailed analytic study of the closed classical orbits and their bifurcations. We then derive a simple form of the uniform semiclassical approximation for the bifurcations that is suitable for an inclusion into a closed-orbit summation. By means of a generalized version of the semiclassical quantization by harmonic inversion, we succeed in calculating high-quality semiclassical spectra for the hydrogen atom in an electric field.

PACS numbers: 32.60.+i,03.65.Sq,31.15.Gy,32.70.Cs

Submitted to: *J. Phys. B: At. Mol. Opt. Phys.*

## 1. Introduction

Because it is classically integrable, the hydrogen atom in a homogeneous electric field can be regarded as the simplest and most fundamental atomic system apart from the field-free hydrogen atom, and consequently the semiclassical treatment of that system is of particular importance. Due to the integrability, of course, the Einstein-Brillouin-Keller torus quantization rules apply, and a semiclassical calculation of photo-absorption spectra based on the existence of quantized classical tori was indeed carried out by Kondratovich and Delos [1, 2].

A more general approach to the semiclassical description of atomic spectra is furnished by closed-orbit theory [3, 4], which is intended to be applicable to atomic systems exhibiting either regular, chaotic or mixed classical behaviour. Therefore, it is of vital interest to see how it can be applied to this apparently simple example.

Closed-orbit theory provides a semiclassical approximation to the quantum response function

$$g(E) = -\frac{1}{\pi} \sum_n \frac{|\langle i|D|n\rangle|^2}{E - E_n + i\epsilon}, \quad (1)$$

which involves the energy eigenvalues  $E_n$  and the dipole matrix elements  $\langle i|D|n\rangle$  connecting the excited states  $n$  to the initial state  $i$ . Semiclassically, the response function splits into a smooth part and an oscillatory part of the form

$$g^{\text{osc}}(E) = \sum_{\text{c.o.}} \mathcal{A}_{\text{c.o.}}(E) e^{iS_{\text{c.o.}}(E)}, \quad (2)$$

where the sum extends over all classical closed orbits starting from the nucleus and returning to it after having been deflected by the external fields.  $S_{\text{c.o.}}$  is the classical action of the closed orbit. The precise form of the recurrence amplitude  $\mathcal{A}_{\text{c.o.}}$  depends on the geometry of the external field configuration [3, 4, 5, 6]. In the presence of a single external field, it reads

$$\mathcal{A}_{\text{c.o.}} = 4\pi \frac{\mathcal{Y}^*(\vartheta_f) \mathcal{Y}(\vartheta_i)}{|m_{12}|} e^{i(\pi/2)\mu} \quad (3)$$

if the orbit is directed along the field axis and

$$\mathcal{A}_{\text{c.o.}} = 2(2\pi)^{3/2} \frac{\sqrt{\sin \vartheta_i \sin \vartheta_f}}{\sqrt{|m_{12}|}} \mathcal{Y}^*(\vartheta_f) \mathcal{Y}(\vartheta_i) \exp\left(i\frac{\pi}{2}\mu + i\frac{\pi}{4}\right) \quad (4)$$

if it is not. Here,  $\vartheta_i$  and  $\vartheta_f$  are the initial and final angles of the trajectory with respect to the field axis,  $\mu$  is its Maslov index, and  $m_{12}$  an element of the monodromy matrix. The function  $\mathcal{Y}(\vartheta)$  encodes the relevant properties of the initial state and the exciting photon. The amplitudes are independent of whether the classical dynamics is regular, chaotic, or mixed. This is in stark contrast to semiclassical trace formulae [7], which represent the quantum density of states as a sum over classical periodic orbits formally analogous to (2), but require different semiclassical amplitudes in the cases of regular or chaotic dynamics. This property makes closed-orbit theory an ideal starting point for a semiclassical quantization of typical atomic systems in external fields.

Nevertheless, even for the simplest of such systems, the hydrogen atom in an electric field, any attempt to semiclassically quantize based on closed-orbit theory so far has been unsuccessful. The reason for this failure is that, even though the closed orbits of the Stark system are easy to describe and classify [8], a multitude of bifurcations exist. Bifurcations of closed orbits lead to a divergence of the semiclassical recurrence amplitudes and thus spoil the semiclassical spectrum. Uniform semiclassical approximations [9, 10, 11] smooth these divergences, but they have so far been restricted to the calculation of low-resolution spectra and have prevented the use of any high-resolution semiclassical quantization scheme. Only recently [12] were we able to introduce a generalization of the semiclassical quantization by harmonic inversion which is capable of coping with uniform approximations. We have chosen the hydrogen atom in an electric field to illustrate our quantization scheme because its closed orbits and their bifurcations can easily be understood and its simplicity makes it a archetypal problem of closed-orbit theory. On the other hand, bifurcations of closed or periodic orbits are a generic phenomenon of mixed regular-chaotic systems, so that their treatment in a semiclassical quantization scheme is an important task with wide-rangig applications. The principal difficulties of this task are already present in the Stark system, so that it furnishes an ideal testing ground for the novel technique.

In [12] we focused on the presentation of the quantization scheme itself. The central theme of the present paper is the classical and semiclassical dynamics of the hydrogen atom in an electric field. In section 2 the classical dynamics of the Stark system is described and the equations of motion are solved explicitly. In section 3,

the closed orbits and their bifurcations are discussed. Semi-analytic formulae for all relevant orbital parameters are derived which have not been given in the literature so far. In section 4, a uniform approximation for the closed-orbit bifurcations in the Stark system is constructed. Although this has been done before [9, 10, 11], we derive our result in a much simpler way as was done previously and bring it into a form that is considerably easier to apply. Section 5 concludes by presenting both low- and high-resolution semiclassical spectra. They prove that uniform approximations can indeed be included into a high-resolution semiclassical quantization. These results solve the long-standing problem of a closed-orbit theory quantization of the Stark effect and serve as a prototype example for the application of the novel method to other systems.

## 2. The equations of motion

If we assume the electric field  $\mathbf{F}$  to be directed along the  $z$ -axis, the Hamiltonian describing the motion of the atomic electron reads, in atomic units,

$$H = \frac{1}{2}\mathbf{p}^2 - \frac{1}{r} + Fz, \quad (5)$$

where  $r^2 = x^2 + y^2 + z^2$ . It can be simplified by means of its scaling properties: If the coordinates and momenta are scaled according to  $\tilde{\mathbf{x}} = F^{1/2}\mathbf{x}$ ,  $\tilde{\mathbf{p}} = F^{-1/4}\mathbf{p}$ , the classical dynamics is found not to depend on the energy  $E$  and the electric field strength  $F$  separately, but only on the scaled energy  $\tilde{E} = F^{-1/2}E$ . In this work, we will use scaled classical quantities throughout in sections 2 and 3, where purely classical calculations are presented. For the sake of simplicity, we will not mark them with a tilde. From section 4 on, the notational distinction between scaled and unscaled quantities will be taken up again.

As is well known [13, 14], the Hamilton-Jacobi equation corresponding to (5) separates in semiparabolic coordinates  $\rho_1, \rho_2, \varphi$ , where

$$\rho_1 = \sqrt{r-z}, \quad \rho_2 = \sqrt{r+z}, \quad (6)$$

and  $\varphi$  is the azimuth angle around the field axis. Notice that  $\rho_1$  and  $\rho_2$  are defined by (6) up to a choice of sign only.

The Hamilton-Jacobi approach leads most naturally to the computation of the action-angle variables fundamental to the EBK quantization. For a discussion of closed orbits, however, it is essential to follow the temporal evolution of a trajectory. This can most conveniently be achieved if the trajectories are parameterized by a parameter  $\tau$  related to the time  $t$  by

$$d\tau = 2r dt. \quad (7)$$

In the following, primes will be used to denote differentiation with respect to  $\tau$ . The Hamiltonian describing the dynamics as a function of  $\tau$  is given by

$$\begin{aligned} \mathcal{H} &= 2r (H - E) \\ &= \frac{1}{2} \left( p_{\rho_1}^2 + p_{\rho_2}^2 + \left( \frac{1}{\rho_1^2} + \frac{1}{\rho_2^2} \right) p_{\varphi}^2 - 2E (\rho_1^2 + \rho_2^2) - \rho_1^4 + \rho_2^4 - 4 \right) = 0. \end{aligned} \quad (8)$$

(See [15] or [5] for a discussion of how to treat the pseudotime transformation (7) within the framework of Hamiltonian dynamics.)

Separating the pseudotime-Hamiltonian (8) into  $\rho_1$ -dependent and  $\rho_2$ -dependent parts and using Hamilton's equation of motion  $\rho'_j = \partial\mathcal{H}/\partial p_{\rho_j} = p_{\rho_j}$ , we obtain

$$\rho_j'^2 = \pm\rho_j^4 + 2E\rho_j^2 - \frac{p_\varphi^2}{\rho_j^2} + c_j \quad \text{for } j = 1, 2 \quad (9)$$

with separation constants  $c_1$  and  $c_2$  related by

$$c_1 + c_2 = 4. \quad (10)$$

Equation (9) can be integrated to yield

$$\tau = \int \frac{d\rho_1}{\sqrt{\rho_1^4 + 2E\rho_1^2 - \frac{p_\varphi^2}{\rho_1^2} + c_1}} = \int \frac{d\rho_2}{\sqrt{-\rho_2^4 + 2E\rho_2^2 - \frac{p_\varphi^2}{\rho_2^2} + c_2}} \quad (11)$$

which gives the parameter  $\tau$  as an elliptic integral in the coordinates  $\rho_1$  and  $\rho_2$ .

In the case of closed orbits,  $p_\varphi = 0$ . At the nucleus, we have  $\rho_j'^2 = c_j$  by (9). The initial conditions for an orbit starting at the nucleus at time  $\tau = 0$  thus read

$$\begin{aligned} \rho_1(0) &= 0, & \rho_2(0) &= 0, \\ \rho_1'(0) &= \sqrt{c_1}, & \rho_2'(0) &= \sqrt{c_2}. \end{aligned} \quad (12)$$

The constants  $c_1$  and  $c_2$  describe the distribution of energy between the uphill and the downhill motion.

According to (9), for real orbits  $\rho_j$  can only assume values which make

$$f_j(\rho_j) = \pm\rho_j^4 + 2E\rho_j^2 + c_j > 0. \quad (13)$$

For the motion in the  $\rho_j$ -direction to be bounded, there must be a real turning point, where  $f_j(\rho_j) = 0$ , because otherwise  $\rho_j$  will keep increasing forever. From the factorized form

$$f_1(\rho_1) = (\rho_1^2 - \rho_{1+}^2)(\rho_1^2 - \rho_{1-}^2), \quad (14)$$

with

$$\rho_{1\pm}^2 = -E \pm \sqrt{E^2 - c_1}, \quad (15)$$

it is obvious that for  $E < 0$  the zeros of  $f_1(\rho_1)$  are real if

$$c_1 < E^2 \quad (16)$$

and complex otherwise. Therefore, a closed orbit can only exist if (16) holds. For energies  $E$  below the Stark saddle energy  $E_S = -2$ , this condition is satisfied for all real orbits because  $c_2 = 4 - c_1 > 0$ . For  $E > E_S$ , there must be a sufficiently strong component of the motion in the uphill direction so that the energy of the downhill motion does not suffice to cross the saddle.

For the  $\rho_2$  motion we obtain similarly

$$f_2(\rho_2) = -(\rho_2^2 - \rho_{2+}^2)(\rho_2^2 - \rho_{2-}^2), \quad (17)$$

with

$$\rho_{2\pm}^2 = E \pm \sqrt{E^2 + c_2}. \quad (18)$$

The coordinate  $\rho_{2+}$  is real for any  $c_2 > 0$ . Therefore, the  $\rho_2$ -motion is always bounded for real orbits.

With the help of the factorizations (14) and (17), the elliptic integrals (11) can easily be reduced to Legendre's standard integral of the first kind [16]

$$\tau = \frac{1}{\rho_+} \mathcal{F} \left( \arcsin \left( \frac{\rho_+}{\sqrt{c_1}} \rho_1 \right) \middle| m_1 \right) = \frac{1}{\rho_-} \mathcal{F} \left( \arcsin \left( \frac{\rho_-}{\sqrt{c_2}} \rho_2 \right) \middle| m_2 \right). \quad (19)$$

The parameters are

$$m_1 = \frac{\rho_{1-}^2}{\rho_{1+}^2} = \frac{c_1}{\rho_+^4}, \quad m_2 = \frac{\rho_{2+}^2}{\rho_{2-}^2} = -\frac{c_2}{\rho_-^4}, \quad (20)$$

and the abbreviations

$$\rho_+ = \rho_{1+}, \quad \rho_- = \sqrt{-\rho_{2-}^2} \quad (21)$$

were introduced. Equation (19) can be solved for  $\rho_1$  and  $\rho_2$  in terms of Jacobi's elliptic functions [16] to yield

$$\begin{aligned} \rho_1(\tau) &= \frac{\sqrt{c_1}}{\rho_+} \operatorname{sn}(\rho_+ \tau | m_1), \\ \rho_2(\tau) &= \frac{\sqrt{c_2}}{\rho_-} \operatorname{sn}(\rho_- \tau | m_2). \end{aligned} \quad (22)$$

These results incorporate the initial conditions (12).

### 3. Closed orbits

Closed orbits are characterized by the condition that at a pseudotime  $\tau_0 > 0$  the electron returns to the nucleus, so that

$$\rho_1(\tau_0) = \rho_2(\tau_0) = 0. \quad (23)$$

In the simplest cases, either  $\rho_1$  or  $\rho_2$  vanishes identically. The electron then moves along the electric field axis.

If  $c_1 = 0$ , the downhill coordinate  $\rho_1$  is zero. The electron leaves the nucleus in the uphill direction, i.e. in the direction of the electric field, until it is turned around by the joint action of the Coulomb and external fields and returns to the nucleus at a pseudotime

$$\tau_2 = 2 \frac{\mathcal{K}(m_2)}{\rho_-}, \quad (24)$$

where  $\mathcal{K}(m)$  denotes the complete elliptic integral of the first kind [16]. Thus,  $\tau_2$  corresponds to a half period of  $\rho_2$  and, due to the freedom in the choice of sign, to a full period of the uphill orbit in position space. The uphill orbit is repeated periodically and closes again at  $\tau_0 = l\tau_1$  with integer  $l$ .

The second case of axial motion is obtained if  $c_1 = 4$ , which corresponds to a downhill motion opposite to the direction of the electric field. The  $\rho_1$  motion closes at pseudotimes  $\tau = k\tau_1$  with

$$\tau_1 = 2 \frac{\mathcal{K}(m_1)}{\rho_+}, \quad (25)$$

if the energy  $E$  is less than the saddle point energy  $E_S = -2$ . If  $E > E_S$ , the electron crosses the Stark saddle and the orbit does not close.

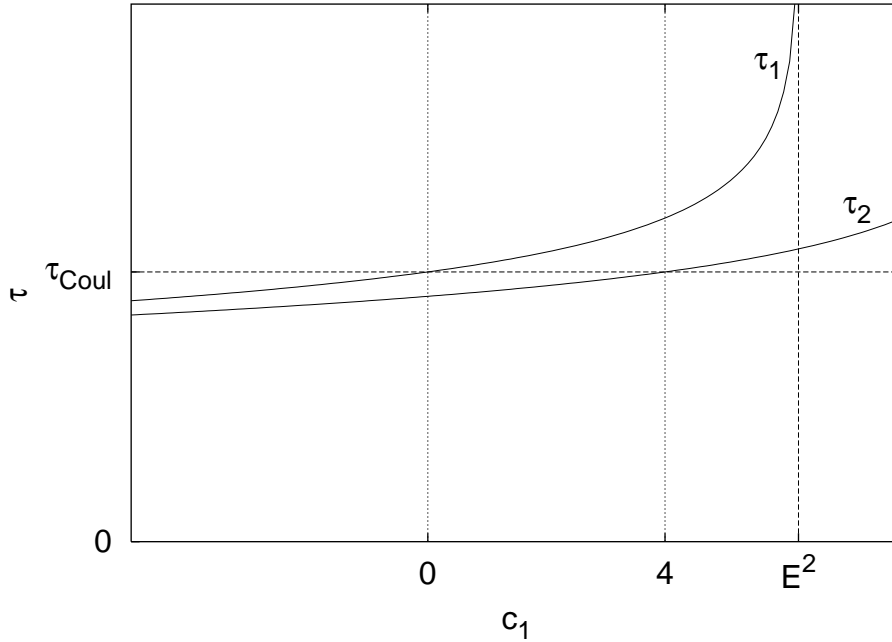


**Figure 1.** Downhill period  $\tau_1$  and uphill period  $\tau_2$  as a function of the separation constant  $c_1$ .

In the case of a non-axial orbit, the uphill and downhill motions must close at the same time

$$\tau_0 = k\tau_1 = l\tau_2 . \quad (26)$$

If (26) is satisfied for any given integer values of  $k$  and  $l$ , the orbit returns to the nucleus after  $k$  half periods of  $\rho_1$  and  $l$  half periods of  $\rho_2$ , corresponding, in Cartesian coordinates, to  $k$  full periods in the downhill and  $l$  full periods in the uphill direction. We therefore refer to  $k$  and  $l$  as the downhill and uphill repetition numbers, respectively, and identify a non-axial closed orbit by its repetition numbers  $(k, l)$ .

If the scaled energy  $E$  is fixed, the half-periods  $\tau_1$  and  $\tau_2$  depend on the separation constant  $c_1$ . For given  $k$  and  $l$ , (26) can therefore be read as an equation for  $c_1$ , thus determining the initial conditions of a closed orbit. We are now going to investigate the solution of this equation to determine the conditions for a  $(k, l)$  orbit to exist.

Figure 1 shows the dependence of  $\tau_1$  and  $\tau_2$  on  $c_1$  for a fixed energy  $E$ . For all  $c_1$ , the uphill period  $\tau_2$  is smaller than the downhill period  $\tau_1$ . Furthermore, as  $c_1 \rightarrow -\infty$  we obtain from (24) and (25), to leading order,

$$\tau_1 - \tau_2 \approx \frac{2\mathcal{K}(-1)}{(-c_1)^{5/4}} , \quad (27)$$

whereas

$$\tau_1 \approx \frac{2\mathcal{K}(-1)}{(-c_1)^{1/4}} , \quad (28)$$

so that the ratio  $\tau_1/\tau_2$  approaches 1 from above. On the other hand,  $\tau_1$  diverges at  $c_1 = E^2$ , so that  $\tau_1/\tau_2 \rightarrow \infty$  as  $c_1 \rightarrow E^2$ . Thus, for any energy  $E < 0$  and positive

	$c_1$	$c_2$	$\rho_1$	$\rho_2$	$m_1$	$m_2$
pre-bifurcation ghost	$c_1 > 4$	$c_2 < 0$	$\in \mathbb{R}$	$\in i\mathbb{R}$	$> 0$	$> 0$
real orbit	$0 \leq c_1 \leq 4$	$0 \leq c_2 \leq 4$	$\in \mathbb{R}$	$\in \mathbb{R}$	$> 0$	$< 0$
post-bifurcation ghost	$c_1 < 0$	$c_2 > 4$	$\in i\mathbb{R}$	$\in \mathbb{R}$	$< 0$	$< 0$

**Table 1.** Comparison of parameter ranges for real and ghost orbits

integers  $k, l$  with  $l > k$ , there is a unique solution  $c_1$  to (26). It is in the range  $-\infty < c_1 < E^2$ . There is no solution for  $l \leq k$ , since  $\tau_1$  is complex for  $c_1 > E^2$  whereas  $\tau_2$  remains real. Therefore, orbits  $(k, l)$  with  $l \leq k$  do not exist.

A real closed orbit must satisfy

$$0 \leq c_1 \leq 4 \quad (29)$$

due to (10) and (12). If (29) is not met, the initial conditions (12) are complex and a ghost orbit in the complexified phase space is obtained. More precisely, if  $c_1 > 4$ , the initial velocity  $\rho'_2(0)$  is imaginary, hence  $\rho_2(\tau)$  will be imaginary at all times. Similarly,  $\rho_1(\tau)$  will be imaginary if  $c_1 < 0$ . In both cases, if the complex conjugate of the ghost orbit is taken, one of the semiparabolic coordinates changes sign. This change of sign does not alter the Cartesian coordinates, and consequently all ghost orbits are invariant with respect to complex conjugation. By the same token, the starting angle of a ghost orbit is defined up to complex conjugation only. We will always choose the imaginary part of starting angles to be positive. The properties of real and ghost orbits are summarized in table 1.

To investigate the bifurcations of the closed orbits, we will now discuss the dependence of  $c_1$  on  $E$  for fixed repetition numbers  $k, l$ . For any energy  $E$  and  $c_1 = 0$ , the downhill period  $\tau_1$  is equal to the period

$$\tau_{\text{Coul}} = \frac{\pi}{\sqrt{-2E}} \quad (30)$$

of the pure Coulomb dynamics. For  $c_1 = 4$ , the uphill period  $\tau_2$  equals  $\tau_{\text{Coul}}$ . For any other value of  $c_1$ , both  $\tau_1$  and  $\tau_2$  converge to  $\tau_{\text{Coul}}$  as  $E \rightarrow -\infty$ , whence in this limit  $\tau_1/\tau_2 \rightarrow 1$ . Thus,  $\tau_1/\tau_2 < l/k$  at  $c_1 = 4$  if  $E$  is sufficiently low. The solution to (26) must then lie in the interval  $c_1 \in [4, E^2]$ , so that the  $(k, l)$ -orbit is a ghost. As  $E$  increases,  $c_1$  decreases. At the critical energy  $E_{\text{gen}}$  where  $c_1 = 4$ , a real  $(k, l)$  orbit is generated. It bifurcates off the downhill orbit that is located at  $c_1 = 4$ . For  $E > E_{\text{gen}}$ ,  $c_1$  decreases further. When the energy  $E_{\text{dest}}$  where  $c_1 = 0$  is reached, the  $(k, l)$  orbit collides with the uphill orbit and becomes a ghost again. As the singularity of  $\tau_1$  approaches zero as  $E \nearrow 0$ , there is an  $E_{\text{dest}} < 0$  for any  $(k, l)$ .

The bifurcation energies  $E_{\text{gen}}$  and  $E_{\text{dest}}$  can be determined from (26) if  $c_1 = 4$  is prescribed for the generation of an orbit, or  $c_1 = 0$  for its destruction. For these cases, equation (26) simplifies to

$$\frac{l}{k} = \frac{2^{3/2}}{\pi \sqrt{1 + \sqrt{1 - \epsilon}}} \mathcal{K} \left( \frac{\epsilon}{(1 + \sqrt{1 - \epsilon})^2} \right) \quad (31)$$

in terms of the dimensionless variable  $\epsilon = 4/E^2 = (E_S/E)^2$  for the generation of the  $(k, l)$  orbit and

$$\frac{k}{l} = \frac{2^{3/2}}{\pi \sqrt{1 + \sqrt{1 + \epsilon}}} \mathcal{K} \left( \frac{-\epsilon}{(1 + \sqrt{1 + \epsilon})^2} \right) \quad (32)$$

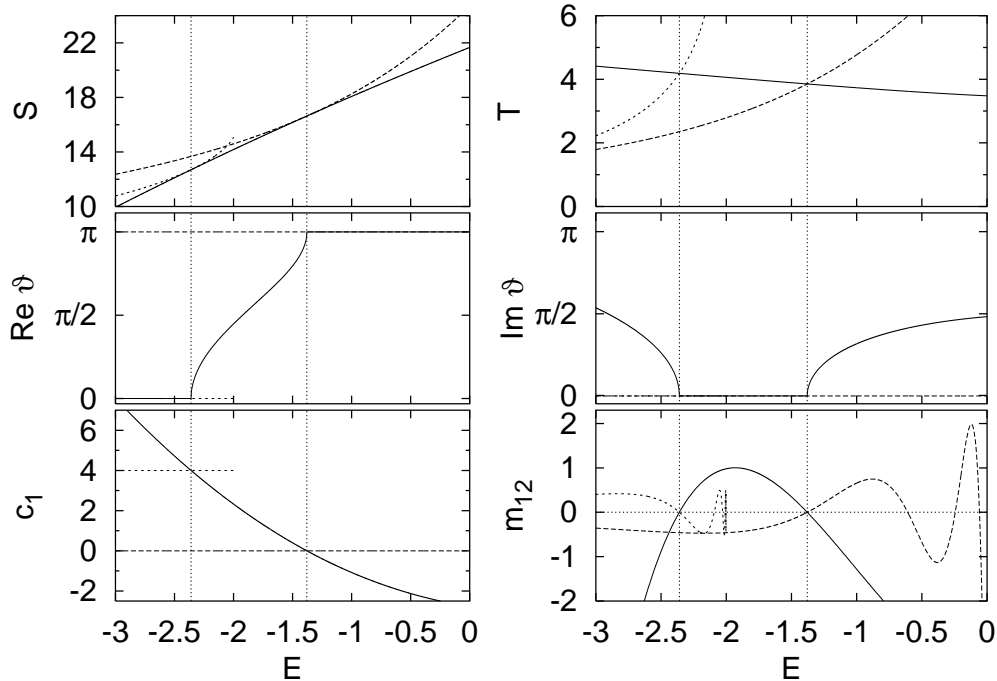


**Figure 2.** Orbital parameters close to the bifurcations of the orbit (4, 5). Solid line: non-axial orbit (4, 5), long-dashed line: fifth uphill orbit, short-dashed line: fourth downhill orbit. Vertical lines indicate the bifurcation energies  $E_{\text{gen}} = -2.3597$  and  $E_{\text{dest}} = -1.3790$ , respectively

for its destruction. These equations provide a simple and stable method to determine the bifurcation energies. They can be expected to yield more accurate results than the numerically computed monodromy matrix elements used by Gao and Delos [8].

The sequence of bifurcations described above is illustrated in figure 2, where characteristic data of the orbit (4, 5), and the downhill and uphill orbits it bifurcates from, is shown. The bifurcation energies  $E_{\text{gen}} = -2.3597$  and  $E_{\text{dest}} = -1.3790$  are characterized by the conditions  $c_1 = 4$  and  $c_1 = 0$ , respectively. The transition between real and ghost orbits can most clearly be seen from the energy dependence of the starting angle  $\vartheta_i$ , which is real between the bifurcation energies and acquires a non-zero imaginary part outside this interval. In addition, at the bifurcation energies the actions and orbital periods of the non-axial orbit coincide with those of the appropriate axial orbits. Note that the action of the non-axial orbit is always smaller than that of the axial orbits.

It is also apparent from figure 2 that the monodromy matrix element  $m_{12}$  vanishes at the bifurcations. For the axial orbits, further zeros of  $m_{12}$  appear in figure 2. They correspond to additional bifurcations these orbits undergo. As  $k < l$  for a non-axial orbit, the  $l$ th repetition of the uphill orbit undergoes  $l-1$  bifurcations, where the orbits  $(k, l)$  with  $k = 1, \dots, l-1$  are destroyed. All four bifurcation energies of the fifth uphill orbit are visible in figure 2. A downhill orbit, on the contrary, undergoes infinitely many bifurcations before it ceases to exist at  $E = -2$ . Only the first members of this infinite cascade are resolved in figure 2.



The separation parameter  $c_1$  for a closed orbit must be calculated numerically from (26). Once it is known, all orbital parameters can be found analytically. The pertinent formulae will now be derived.

First of all, if we transform the orbits (22) to Cartesian coordinates, we find that the starting and returning angle  $\vartheta$  of a closed orbit, measured with respect to the field axis, is related to the separation constants by

$$2 \cos \frac{\vartheta}{2} = \sqrt{c_1}, \quad 2 \sin \frac{\vartheta}{2} = \sqrt{c_2}, \quad (33)$$

so that

$$\vartheta = 2 \arccos \frac{\sqrt{c_1}}{2}. \quad (34)$$

The angle  $\vartheta$  determined from (34) is obviously real and confined to the interval  $0 \leq \vartheta \leq \pi$  if  $0 \leq c_1 \leq 4$ , as was to be expected for a real orbit. For a pre-bifurcation ghost orbit, i.e.  $c_1 > 4$ , the equations (33) can be satisfied if  $\vartheta = i\alpha$  is chosen purely imaginary with

$$2 \cosh \frac{\alpha}{2} = \sqrt{c_1}, \quad 2i \sinh \frac{\alpha}{2} = \sqrt{c_2}. \quad (35)$$

This choice of  $\vartheta$ , which is unique up to the addition of multiples of  $4\pi$ , makes  $\vartheta$  continuous at the bifurcation. Similarly, for  $c_1 < 0$ , i.e. for a post-bifurcation ghost orbit, we set  $\vartheta = \pi + i\alpha$  with

$$2i \sinh \frac{\alpha}{2} = \sqrt{c_1}, \quad 2 \cosh \frac{\alpha}{2} = \sqrt{c_2}. \quad (36)$$

Again, the real part makes  $\vartheta$  continuous at the bifurcation. In both cases we assume  $\alpha > 0$ , which is possible because the orbit is invariant under complex conjugation.

Using  $p_{\rho_j} = \rho'_j$ , we obtain the action integral

$$\begin{aligned} S &= \int p_{\rho_1} d\rho_1 + \int p_{\rho_2} d\rho_2 \\ &= 2k \int_0^{\sqrt{c_1}/\rho_+} \rho'_1 d\rho_1 + 2l \int_0^{\sqrt{c_2}/\rho_-} \rho'_2 d\rho_2. \end{aligned} \quad (37)$$

The equations of motion (9) then yield

$$\begin{aligned} S &= 2k \int_0^{\sqrt{c_1}/\rho_+} \sqrt{f_1(\rho_1)} d\rho_1 + 2l \int_0^{\sqrt{c_2}/\rho_-} \sqrt{f_2(\rho_2)} d\rho_2 \\ &= \frac{2}{3} k \rho_+^3 I(m_1) - \frac{2}{3} l \rho_-^3 I(m_2) \end{aligned} \quad (38)$$

with

$$I(m) = (m-1)\mathcal{K}(m) + (m+1)\mathcal{E}(m) \quad (39)$$

and the complete elliptic integrals of the first and second kinds  $\mathcal{K}(m)$  and  $\mathcal{E}(m)$  [16]. Note that  $I(m) < 0$  if  $m < 0$ , so that both terms in (38) are positive for real orbits. For a downhill orbit, the uphill repetition number  $l$  is undefined. As, however, in this case  $m_2 = 0$  and  $I(0) = 0$ , the uphill contribution drops out of (38) for a downhill orbit. Similarly, the downhill contribution vanishes for uphill orbits. The action  $S$  given by (38) is real for both real and ghost orbits.

The physical-time period of a closed orbit is given by

$$\begin{aligned} T &= \int_0^{\tau_0} \rho_1^2 d\rho_1 + \int_0^{\tau_0} \rho_2^2 d\rho_2 \\ &= 2k\rho_+ (\mathcal{K}(m_1) - \mathcal{E}(m_1)) - 2l\rho_- (\mathcal{K}(m_2) - \mathcal{E}(m_2)). \end{aligned} \quad (40)$$

As is the action, the period  $T$  is always real.

The calculation of the monodromy matrix element  $m_{12}$  is more difficult. It proceeds from the  $2 \times 2$  Jacobian matrix

$$J = \frac{\partial \rho(\tau_0)}{\partial \mathbf{p}(0)} \quad (41)$$

that describes the change of the final position upon a variation of the initial momentum. The initial and final momenta are given by

$$\mathbf{p}(0) = \begin{pmatrix} \sqrt{c_1} \\ \sqrt{c_2} \end{pmatrix}, \quad \mathbf{p}(\tau_0) = \begin{pmatrix} (-1)^k \sqrt{c_1} \\ (-1)^l \sqrt{c_2} \end{pmatrix}, \quad (42)$$

They have norm 2 by (10). As the monodromy matrix characterizes variations perpendicular to the orbit,  $m_{12}$  is obtained from  $J$  by projecting onto unit vectors perpendicular to the momenta (42). Thus,

$$m_{12} = \frac{1}{2} \left( (-1)^l \sqrt{c_2}, -(-1)^k \sqrt{c_1} \right) \cdot J \cdot \frac{1}{2} \begin{pmatrix} \sqrt{c_2} \\ -\sqrt{c_1} \end{pmatrix}. \quad (43)$$

Since the dynamics is separable, the matrix  $J$  is diagonal, whence

$$m_{12} = (-1)^l \frac{c_2}{4} \left. \frac{\partial \rho_1(\tau)}{\partial p_1(0)} \right|_{\tau=\tau_0} + (-1)^k \frac{c_1}{4} \left. \frac{\partial \rho_2(\tau)}{\partial p_2(0)} \right|_{\tau=\tau_0}. \quad (44)$$

For the remaining derivatives we find from (22)

$$\frac{\partial \rho_1(\tau)}{\partial p_1(0)} = \left( \frac{\partial}{\partial p_1(0)} \frac{\sqrt{c_1}}{\rho_+} \right) \text{sn}(\rho_+ \tau | m_1) + \frac{\sqrt{c_1}}{\rho_+} \frac{\partial}{\partial p_1(0)} \text{sn}(\rho_+ \tau | m_1). \quad (45)$$

A similar expression holds for  $\rho_2$ . If a non-axial orbit  $(k, l)$  is considered, the first term in (45) vanishes at  $\tau = \tau_0$  by virtue of the resonance condition (26). The second term can be evaluated in an elementary, but lengthy calculation to yield

$$\begin{aligned} m_{12} = & (-1)^{k+l} \frac{km_1 c_2}{4\rho_+ \sqrt{E^2 - c_1}} (2Ed(m_1) - \rho_+^2 \mathcal{K}(m_1)) \\ & + (-1)^{k+l} \frac{lm_2 c_1}{4\rho_- \sqrt{E^2 + c_2}} (2Ed(m_2) - \rho_-^2 \mathcal{K}(m_2)) \end{aligned} \quad (46)$$

with

$$d(m) = \frac{\mathcal{E}(m)}{m(1-m)} - \frac{\mathcal{K}(m)}{m}. \quad (47)$$

From (46) it can be verified that, up to a choice of sign, the matrix element  $m_{12}$  for the orbit  $(nk, nl)$ , which is the  $n$ th repetition of  $(k, l)$ , equals  $n$  times the matrix element for the orbit  $(k, l)$ , as has been shown previously by Gao and Delos [8] by an abstract argument using the neutral stability of the orbits. It is also clear from (46) that  $m_{12}$  vanishes when the orbit undergoes a bifurcation, because  $m_1 \rightarrow 0$  as  $c_1 \rightarrow 0$ , and  $\mathcal{K}(m_1)$  and  $d(m_1)$  both approach finite limits.

For an uphill orbit the second term in (45) vanishes because  $c_1 = 0$ , whereas the first term is nonzero in general because the axial orbits do not obey a resonance condition akin to (26). The derivative reads

$$\left. \frac{\partial \rho_1(\tau)}{\partial p_1(0)} \right|_{c_1=0} = \frac{\sin(\sqrt{-2E} \tau)}{\sqrt{-2E}}, \quad (48)$$

so that

$$m_{12} = (-1)^l \frac{\sin(\sqrt{-2E} \tau_0)}{\sqrt{-2E}}. \quad (49)$$

Similarly, the matrix element for a downhill orbit is

$$m_{12} = (-1)^k \frac{\sin(\sqrt{-2E} \tau_0)}{\sqrt{-2E}}. \quad (50)$$

Finally, the Maslov indices of the closed orbits need to be determined. For the uphill orbits, we proceed as follows: First, there is a caustic whenever the orbit reaches either the nucleus or the turning point, totalling to  $2l - 1$  caustics. Second, the Maslov index increases by two (corresponding to two independent directions transverse to the orbit) whenever the orbit is intersected by neighbouring trajectories, i.e. when (48) vanishes. This occurs, by (48), after a pseudotime  $\tau_{\text{Coul}}$ , so that the intersections contribute  $2[\tau_0/\tau_{\text{Coul}}]$  to the Maslov index.  $[x]$  denotes the integer part of  $x$ . Third, if the semiclassical amplitudes are written according to the conventions of [5, 6], the Maslov index must be increased by one, so that for an uphill orbit it finally reads

$$\mu = 2 \left( l + \left[ \frac{l\tau_2}{\tau_{\text{Coul}}} \right] \right). \quad (51)$$

Using the same reasoning, we find

$$\mu = 2 \left( k + \left[ \frac{k\tau_1}{\tau_{\text{Coul}}} \right] \right), \quad (52)$$

for a downhill orbit. As the downhill period  $\tau_1$  is always larger than  $\tau_{\text{Coul}}$ , the downhill Maslov index (52) is equal to  $4k$  for sufficiently low  $E$ .

The Maslov index of a non-axial orbit involves the number of zeros of  $m_{12}$  encountered along the orbit, which is hard to find from (22). Instead, we exploit the observation that the change of Maslov indices in a bifurcation can be determined from the normal form describing the bifurcation. A normal form suitable for the bifurcations in the Stark effect will be given in section 4. It predicts that in a bifurcation the Maslov index of the axial orbit increases by two, which is consistent with (51) and (52), and the Maslov index of the non-axial orbit takes the intermediate value. A schematic drawing of the shortest orbits and their bifurcations is shown in figure 3. It implies that the Maslov index of a non-axial orbit is

$$\mu = 2(k + l) - 1. \quad (53)$$

Since along the orbit there are  $k - 1$  zeros of  $\rho_1$  and  $l - 1$  zeros of  $\rho_2$ , each corresponding to an intersection with the electric field axis and thus contributing 1 to the Maslov index, there must be  $k + l - 1$  zeros of  $m_{12}$ . This result can be confirmed numerically.

For ghost orbits, Maslov indices cannot be determined by counting caustics. The correct phase of the ghost orbit contribution is fixed by demanding that the semiclassical amplitude be continuous across the bifurcations, as required by the uniform approximation to be developed below.

#### 4. The uniform approximation

In the following sections we present the semiclassical treatment of the Stark effect. From now on, scaled quantities will again be marked with a tilde.

It has become clear in section 3 that the apparently simple dynamics of the hydrogen atom in an electric field contains numerous bifurcations of closed orbits.

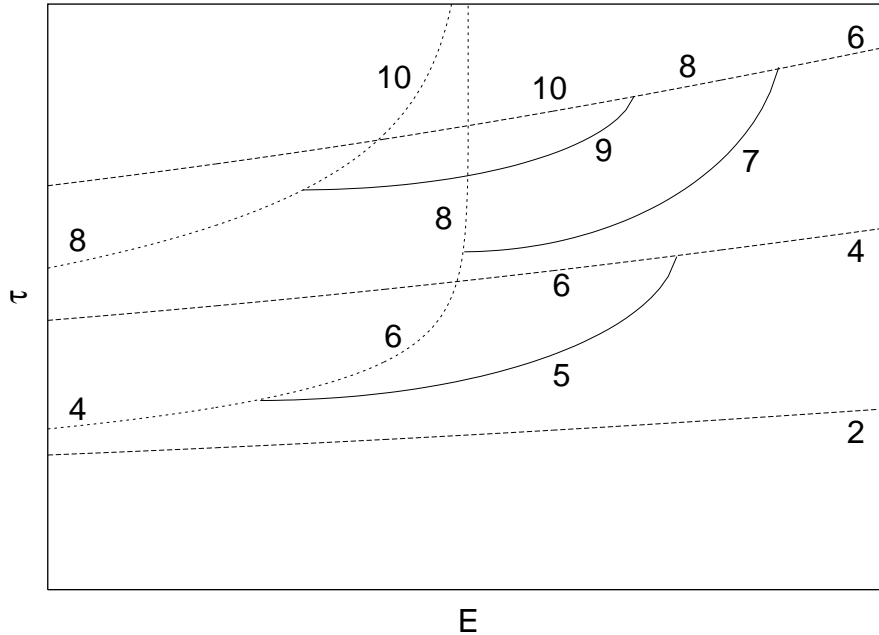


**Figure 3.** Periods of the shortest closed orbits, labelled by their Maslov indices, as a function of energy (schematic). Solid lines: non-axial orbits, short-dashed lines: downhill orbits, long-dashed lines: uphill orbits.

They lead to zeros of the monodromy matrix elements  $m_{12}$  of the bifurcating orbits and thus to the divergence of the pertinent closed-orbit amplitudes (4), so that they spoil the semiclassical spectrum (see section 5). To overcome this problem, a uniform semiclassical approximation giving the collective contribution of the bifurcating orbits must be derived. For the bifurcations occurring in the hydrogen atom in an electric field, this was done by Gao and Delos [9]. These authors constructed a semiclassical wave function near a bifurcation and essentially redid the derivation of closed-orbit theory using that wave function. Their uniform approximation was extended by Shaw and Robicheaux [10, 11] to include ghost orbits.

In the form given in [9, 10, 11], the uniform approximation cannot be calculated from the actions and recurrence amplitudes characterizing the bifurcating orbits, but requires the determination of additional parameters. It is therefore hard to apply if many closed-orbit bifurcations are to be dealt with. In this section we will present a novel approach to uniformizing the bifurcations in the Stark system that is not only simpler than previous derivations, but also yields the uniform approximation in a more convenient form. It will be shown that only the actions recurrence strengths of the isolated orbits are needed to compute a uniform approximation. This makes the uniform approximation as easy to use as the simple isolated-orbits formula.

The crucial step in the construction of a uniform approximation is the choice of a suitable ansatz function whose stationary points describe the classical closed orbits. In the Stark system, the structure of the bifurcations is determined by the rotational symmetry of the system. Non-axial orbits occur in one-parameter families generated by the rotation of any particular member around the electric field axis, whereas the

axial orbit is isolated at all energies except at a bifurcation. The normal form must share these symmetry properties.

We choose the normal form  $\Phi$  to be defined on a plane with Cartesian coordinates  $(x, y)$  or polar coordinates

$$x = r \cos \varphi, \quad y = r \sin \varphi. \quad (54)$$

Due to the rotational symmetry,  $\Phi$  must be a function of the radial coordinate  $r$  only, independent of the angle  $\varphi$ . To be a smooth function of  $x$  and  $y$ , it must be a function of  $r^2$ . Any such function has a stationary point at the origin  $x = y = 0$  that corresponds to the axial orbit because it is rotation invariant. Any stationary point at a non-zero radial coordinate  $r_c$  occurs on a ring  $r = r_c$  and describes a family of non-axial orbits. A normal form suitable to describe the bifurcations occurring in the Stark system must therefore have stationary points on a ring with radius  $r_c$  that shrinks to zero as the bifurcation is approached.

These requirements are fulfilled by the normal form

$$\Phi_a(x, y) = \frac{1}{4} r^4 - \frac{1}{2} a r^2 \quad (55)$$

with a real parameter  $a$ . Apart from the trivial stationary point at the origin, (55) has a ring of stationary points at  $r = \sqrt{a}$ , which is real if  $a > 0$  and imaginary if  $a < 0$ . Thus, (55) describes a family of non-axial real orbits present for  $a > 0$  which then contracts onto an axial orbit and becomes a family of ghost orbits.

For the uniform approximation we make the ansatz

$$\Psi(E) = I(a) e^{i S_{\text{ax}}(E)}, \quad (56)$$

where  $S_{\text{ax}}(E)$  denotes the action of the axial orbit and

$$I(a) = \int dx dy p(x^2 + y^2) e^{i \Phi_a(x, y)}, \quad (57)$$

with an arbitrary smooth rotationally symmetric function  $p(r^2)$ . The parameter  $a$  and the function  $p(r^2)$  must now be determined such that, when the distance from the bifurcation gets large, the uniform approximation reproduces the isolated-orbits formula. The asymptotic behaviour of (56) can be found if (57) is evaluated in the stationary-phase approximation. The contribution of the stationary point at the origin is straight-forward to evaluate. It yields

$$I(a)|_{r=0} = \frac{2\pi i}{|a|} p(0) e^{-i \frac{\pi}{2} \nu_0} = -\frac{2\pi i}{a} p(0), \quad (58)$$

where

$$\nu_0 = \begin{cases} 0 & : a < 0 \\ 2 & : a > 0 \end{cases} \quad (59)$$

is the number of negative eigenvalues of the Hessian matrix. From this number it is apparent that the Maslov index of the axial orbit increases by 2 in the bifurcation.

The contribution of the non-axial orbits is present if  $a > 0$ . Due to the rotational symmetry, a straight-forward stationary-phase approximation to this contribution fails because the stationary points are not isolated. In polar coordinates, the integration over the angle  $\varphi$  yields the constant  $2\pi$ , and the stationary-phase approximation can be applied to the remaining integral over  $r$ . This yields

$$I(a)|_{\text{ring}} = 2\pi \sqrt{\pi i} p(a) e^{-i a^2/4}. \quad (60)$$

Note that the contribution of the non-axial orbit remains finite as  $a \rightarrow 0$ .

Thus, the uniform approximation (56) asymptotically equals

$$\Psi(E) \approx -\frac{2\pi i}{a} p(0) e^{iS_{\text{ax}}(E)} + 2\pi\sqrt{\pi i} p(a) e^{i(S_{\text{ax}}(E)-a^2/4)}. \quad (61)$$

This result should reproduce the isolated-orbits formula

$$\mathcal{A}_{\text{ax}}(E) e^{iS_{\text{ax}}(E)} + \mathcal{A}_{\text{non}}(E) e^{iS_{\text{non}}(E)} \quad (62)$$

in terms of the actions and recurrence amplitudes of the axial and non-axial orbits. This can be achieved if we demand

$$S_{\text{non}} = S_{\text{ax}} - a^2/4, \quad (63)$$

$$\mathcal{A}_{\text{ax}} = -\frac{2\pi i}{a} p(0), \quad \mathcal{A}_{\text{non}} = 2\pi\sqrt{\pi i} p(a). \quad (64)$$

The normal form parameter

$$a = \pm 2\sqrt{S_{\text{ax}} - S_{\text{non}}} \quad (65)$$

can be determined from (63). The sign of  $a$  has to be chosen according to whether the non-axial orbits are real or complex.

In the limit  $a \rightarrow 0$ , i.e. close to the bifurcation,  $p(a) \approx p(0)$ . Equation (64) thus imposes the constraint

$$\frac{1+i}{\sqrt{2\pi}} \mathcal{A}_{\text{non}} = -a\mathcal{A}_{\text{ax}} \quad (66)$$

on the semiclassical amplitudes. Note that both sides of this equation are finite as  $a \rightarrow 0$ . In particular,  $\mathcal{A}_{\text{non}}$  is continuous at  $a = 0$ . This condition was used in section 3 to fix the Maslov indices for the ghost orbits. The actual semiclassical amplitudes satisfy (66) close to the bifurcation, but the agreement is satisfactory in the immediate neighbourhood of the bifurcation only.

For  $p(r^2)$  in equation (57) we choose a first-order polynomial

$$p(r^2) = p_0 + p_1(r^2 - a) \quad (67)$$

for the amplitude function. The coefficients  $p_0$  and  $p_1$  are chosen to satisfy (64):

$$p_0 = \frac{\mathcal{A}_{\text{non}}}{\sqrt{2\pi}\pi(1+i)}, \quad p_1 = \frac{1}{2\pi i a} \left( a\mathcal{A}_{\text{ax}} + \frac{1+i}{\sqrt{2\pi}} \mathcal{A}_{\text{non}} \right). \quad (68)$$

By (66),  $p_1$  remains finite at the bifurcation. Thus, the uniform approximation (56) assumes the form

$$\Psi(E) = \left[ \frac{\mathcal{A}_{\text{non}}}{(1+i)} I_0 + \frac{1}{a} \left( a\mathcal{A}_{\text{ax}} + \frac{1+i}{\sqrt{2\pi}} \mathcal{A}_{\text{non}} \right) I_1 \right] e^{iS_{\text{ax}}} \quad (69)$$

with the integrals

$$I_0 = \frac{1}{2^{1/2}\pi^{3/2}} \int dx dy e^{i\Phi_a(x,y)}, \quad I_1 = \frac{1}{2\pi i} \int dx dy (r^2 - a) e^{i\Phi_a(x,y)}. \quad (70)$$

$I_0$  can be evaluated in terms of the Fresnel integrals [16]

$$C(x) = \int_0^x \cos\left(\frac{\pi}{2} t^2\right) dt, \quad S(x) = \int_0^x \sin\left(\frac{\pi}{2} t^2\right) dt \quad (71)$$

to yield

$$I_0 = e^{-ia^2/4} \left[ \frac{1+i}{2} - C\left(-\frac{a}{\sqrt{2\pi}}\right) - iS\left(-\frac{a}{\sqrt{2\pi}}\right) \right]. \quad (72)$$

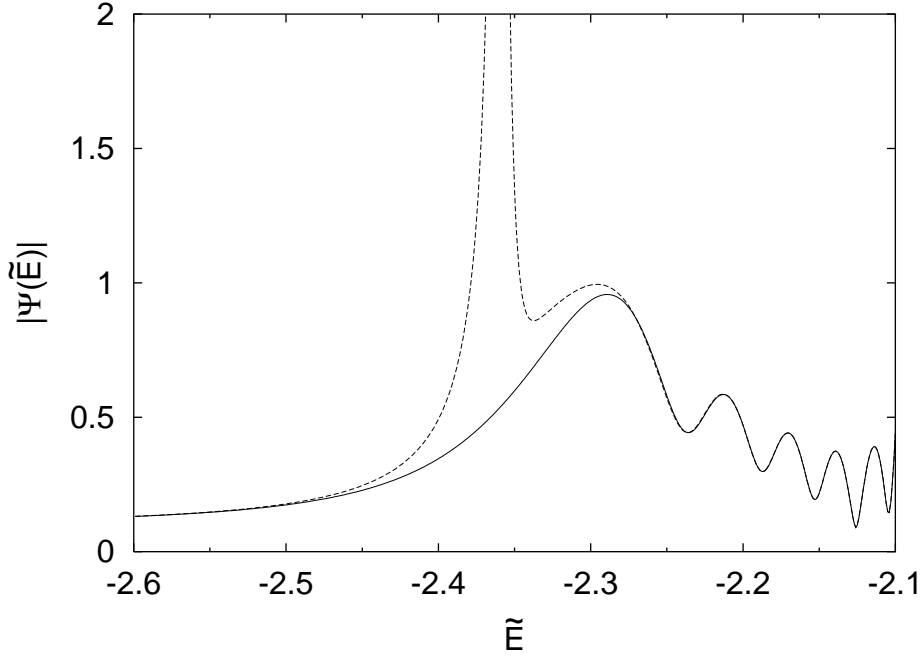


**Figure 4.** Uniform approximation for the generation of the (4,5) non-axial orbit from the downhill orbit for the electric field strength  $F = 10^{-8}$ . Solid line: Uniform approximation (69), dashed line: isolated-orbits approximation.

$I_1$  can be reduced to

$$I_1 = \frac{1}{2i} e^{-ia^2/4} \int_{-a}^{\infty} dv v e^{iv^2/4} \quad (73)$$

with  $v = r^2 - a$ . The integral in (73) diverges at  $v = \infty$ . It can be regularized by adding a small exponential damping factor  $e^{-\varepsilon v^2}$  and letting  $\varepsilon \rightarrow 0$  at the end. This procedure yields

$$I_1 = 1. \quad (74)$$

The regularization can be justified by noting that the stationary phase approximation to (70) also yields  $I_1 = 1$ , so that (74) has the required asymptotic behaviour.

The calculation of the uniform approximation (56) is thus finished. As an example, the uniform approximation for the bifurcation of the (4,5) non-axial orbit off the downhill orbit is compared to the simple closed-orbit formula in figure 4. Obviously, the uniform approximation (69) smooths the divergence of the isolated-orbits approximation and, as desired, asymptotically reproduces the simple approximation perfectly.

## 5. Semiclassical spectra

A low-resolution semiclassical photo-absorption spectrum can be obtained from the closed-orbit sum (2) by including orbits with an orbital period up to a maximum  $T_{\max}$  only. In order to resolve individual energy levels,  $T_{\max}$  must be larger than the

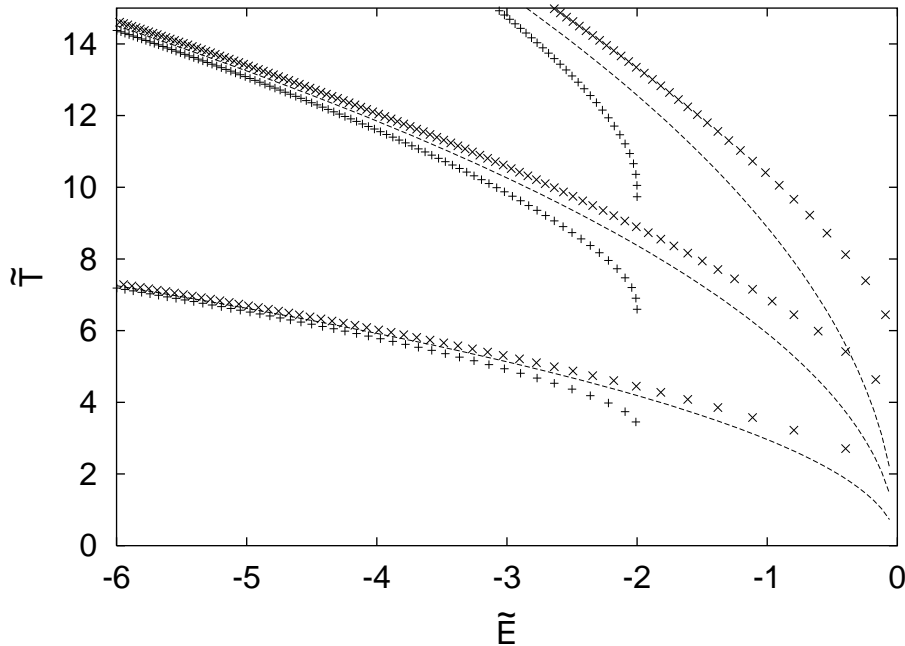


**Figure 5.** Bifurcations of non-axial orbits off the downhill (+) and uphill (x) orbits in a scaled period vs. scaled energy plot. Bifurcation energies and scaled periods of the bifurcating orbits are indicated. Dashed lines: single, double and triple scaled perturbative Heisenberg time (75).

Heisenberg time  $T_H$ . A rough estimate for  $T_H$  can be obtained from perturbation theory. To first order in the electric field strength, the energy splitting between two adjacent spectral lines with principal quantum number  $n$  is [13]  $\Delta E_p = 3nF$ , so that the scaled perturbative Heisenberg time is

$$\tilde{T}_{H,p} = \frac{2\pi F^{3/4}}{\Delta E_p} = \frac{2\pi}{3} \sqrt{-2\tilde{E}}. \quad (75)$$

This estimate is reasonable (although it may not be quantitatively precise) as long as different  $n$ -manifolds do not overlap. If they do, the mean level spacing is much smaller and the Heisenberg time therefore much larger than given by (75).

Multiples of the scaled perturbative Heisenberg time (75) are plotted in figure 5 together with the scaled energies and scaled periods of bifurcating orbits. For low scaled energies, the periods of bifurcating orbits are well approximated by  $\tilde{T}_{H,p}$ . Therefore, there is no parameter range where the closed-orbit sum can be extended up to the Heisenberg time without involving bifurcations, so that the uniformization of bifurcations must be an essential ingredient to any closed-orbit theory quantization of the Stark effect.

These findings can be confirmed numerically. Figure 6 displays the oscillatory part of the photo-absorption cross section as calculated from the closed-orbit sum. All spectra presented in this section are non-scaled spectra calculated for the hydrogen atom in an electric field  $F = 10^{-8} \hat{=} 51.4 \text{V/cm}$ , corresponding to  $w = 100$  and  $\tilde{E} = 10^4 E$ , with the initial state  $|1s\rangle$  and light linearly polarized along the electric



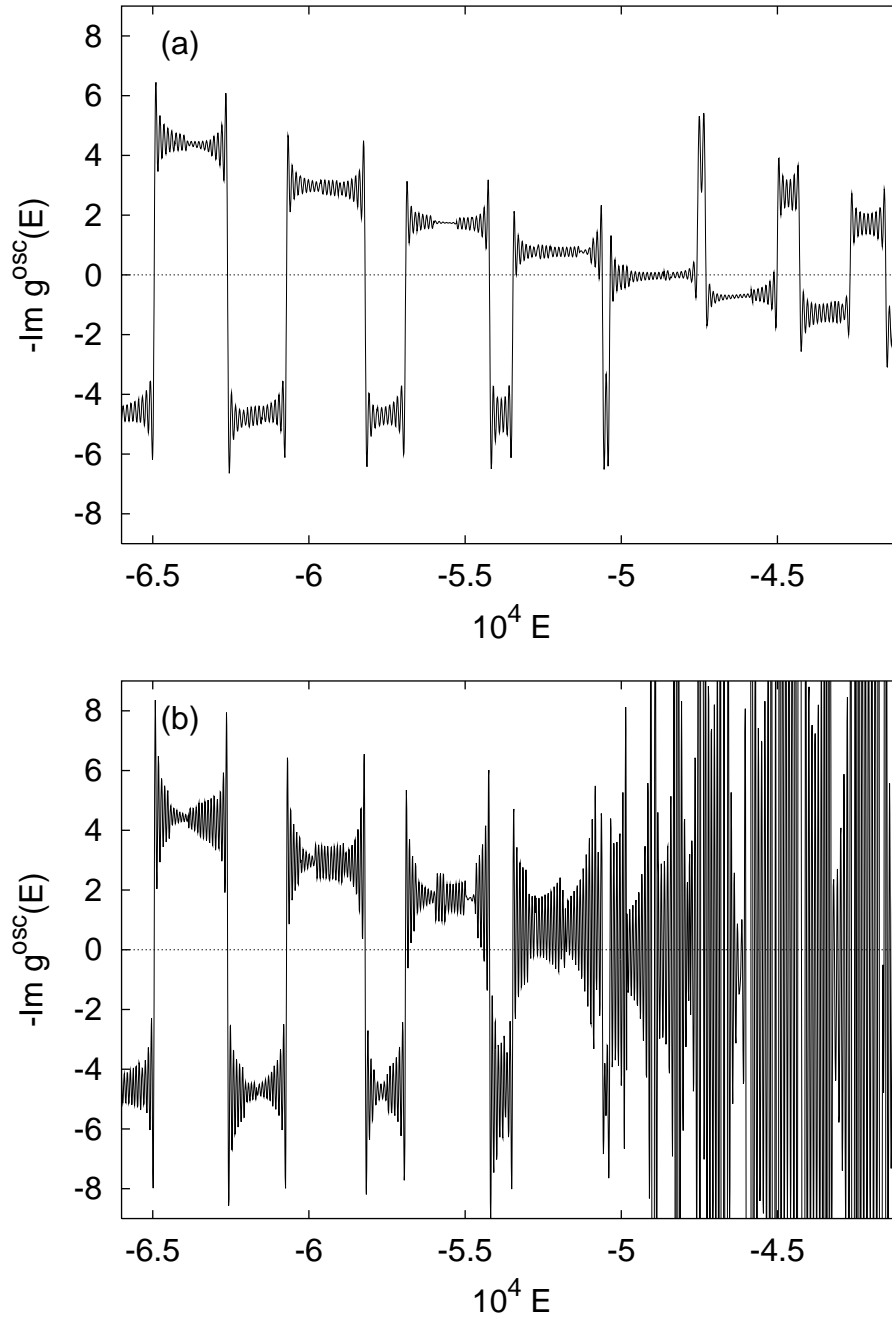


**Figure 6.** Closed-orbit sum without uniform approximations as a function of energy at the electric field strength of  $F = 10^{-8}$  with scaled cut-off time (a)  $\tilde{T}_{\text{max}} = 5$ , (b)  $\tilde{T}_{\text{max}} = 6.5$ . At  $E > -5 \times 10^{-4}$ , the latter is dominated by bifurcation-induced divergences.

field axis. Small discontinuities are introduced in the low-resolution spectra because a closed orbit abruptly disappears from the truncated sum when its period increases beyond the chosen cut-off time  $\tilde{T}_{\max}$ . The discontinuities can be avoided by choosing a smooth cut-off function to gradually switch off the contribution of an orbit when its period approaches the cut-off time. The changes in the spectra are hardly visible, and as excellent results can be obtained with the simple hard cut-off, no smoothing will be used henceforth.

For the spectrum in figure 6(a), a scaled cut-off time of  $\tilde{T}_{\max} = 5$ , well below the perturbative Heisenberg time, was chosen. Consequently, one can distinguish groups of levels characterized by a fixed principal quantum number  $n$ , but no individual spectral lines can be resolved in the plot. The small oscillations are an artefact of the closed-orbit sum and cannot be identified with spectral lines. This is clear from the observations that the frequency of the oscillation increases with increasing cut-off time and that virtually the same oscillations are visible within an  $n$ -manifold and between manifolds.

At low energies, different  $n$ -manifolds do not overlap, so that spectral regions with high oscillator strength density alternate with regions where no spectral lines are present. (As the smooth part of the semiclassical spectrum has been omitted, the bottom line of the semiclassical spectrum is shifted to negative values of the oscillator strength density.) At  $E \approx -4.7 \times 10^{-4}$ , neighbouring  $n$ -manifolds start to overlap. In the overlap regions the spectral density is considerably higher than in regions of isolated  $n$ -manifolds.

To improve the resolution, the cut-off time must be increased. Figure 6(b) displays the results for a scaled cut-off time of  $\tilde{T}_{\max} = 6.5$ . At low energies, this is still below the perturbative Heisenberg time, and no significant improvement of the resolution can be found. At high energies, bifurcations start to occur, and a dense sequence of bifurcation-induced divergences covers the semiclassical signal. As the cut-off time is further increased, bifurcations occur at ever lower energies and destroy ever larger parts of the semiclassical spectrum. It is thus obvious that in its simple form the closed-orbit sum is useless for a complete quantization.

If, on the contrary, the uniform approximations are included, the closed-orbit sum can be extended to longer orbits. Figure 7 shows the uniformized closed-orbit sum for a scaled cut-off time  $\tilde{T}_{\max} = 15$ . As will also be done in all subsequent semiclassical spectra, the uniform approximation was applied for bifurcating orbits whose action difference is less than  $2\pi$ . If for a given orbit several other orbits satisfy this requirement, a more complicated uniform approximation describing several bifurcations should be used (see the discussion at the end of section 5). For the time being, we resolve this conflict by calculating the simple uniform approximation for the two orbits with the smallest action difference and treating all other orbits as isolated.

Although individual spectral lines can be discerned in figure 7, it would be hard to obtain precise values of the energy levels and, in particular, of the associated dipole matrix elements from this figure. A more reliable method of extracting the spectral information from the semiclassical data is clearly desirable. To this end, we will use the method of semiclassical quantization by harmonic inversion [17, 18, 19], which we recently generalized to be applicable in connection with uniform approximations [12]. This method requires the cut-off time of the closed orbit sum to be chosen larger than twice the Heisenberg time for this purpose. The perturbative Heisenberg time thus suggests that a scaled cut-off time of  $\tilde{T}_{\max} = 15$  will be sufficient as long as different  $n$ -manifolds do not overlap. Figure 8 presents the energy levels and transition matrix

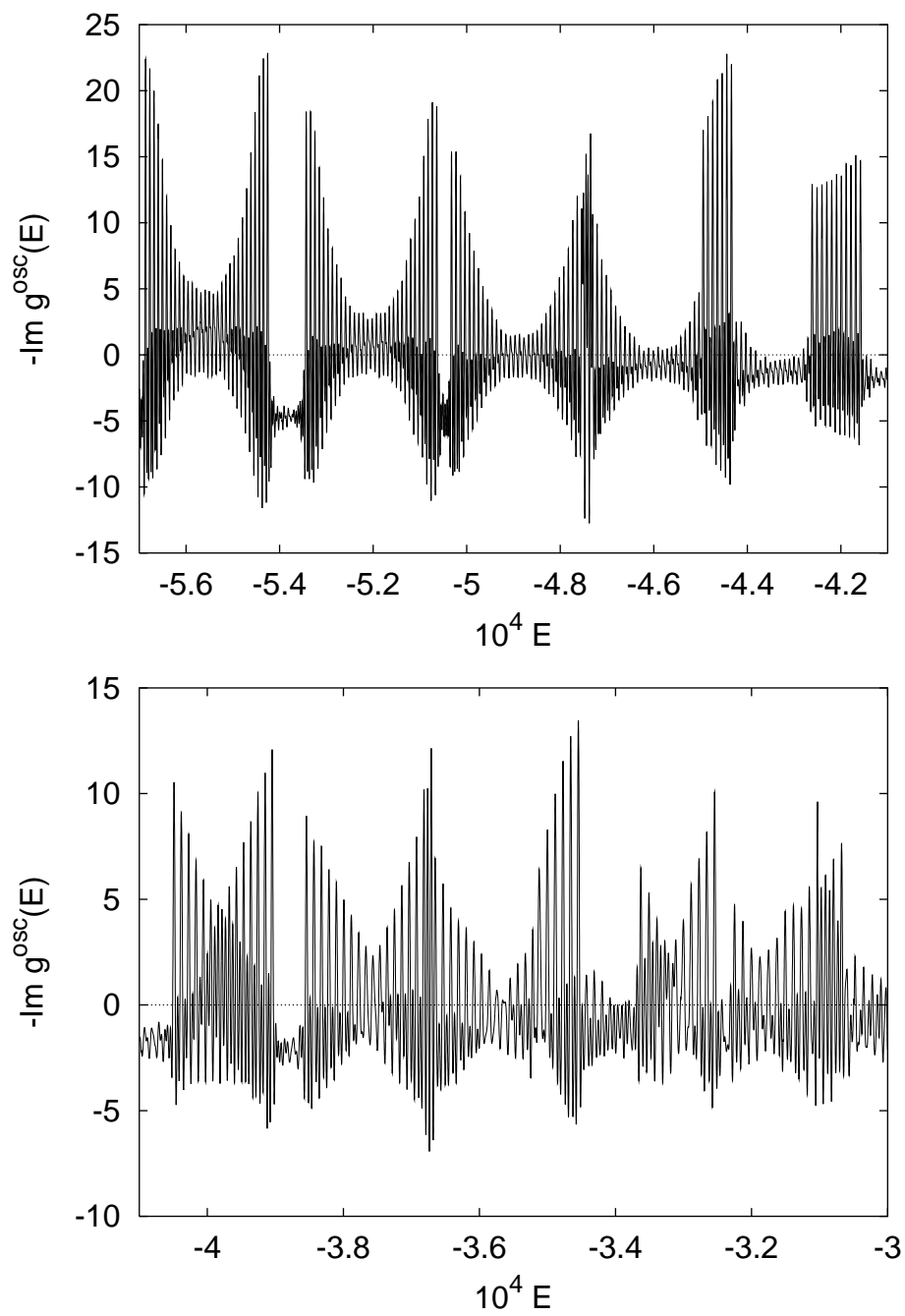


Figure 7. Low-resolution semiclassical spectrum with scaled cut-off time  $\tilde{T}_{\text{max}} = 15$ .

elements obtained from it by the harmonic inversion procedure and compares them to the exact quantum results.

In the region of isolated  $n$ -manifolds the quantum and semiclassical spectra can indeed be compared line by line to reveal excellent agreement in both the position and the intensity of spectral lines. Note, in particular, that the low-resolution semiclassical spectrum apparently ascribes considerable amplitudes to spectral lines in the middle of an  $n$ -manifold, whereas the quantum amplitudes nearly vanish. The high-resolution semiclassical spectrum correctly identifies these amplitudes as being very small. Furthermore, it can be seen from the magnified low-resolution spectrum of the manifold  $n = 31$  in figure 9(a) that the spectral lines, in particular the weak lines close to the centre of the manifold, appear asymmetric in shape in the semiclassical spectrum: They extend farther to the right than to the left. Nevertheless, the high-resolution analysis identifies the lines correctly.

Figure 9(b) shows the low-resolution spectrum for the manifold  $n = 31$  with a signal length of  $\tilde{T}_{\max} = 40$ . It can be seen that the spectral lines close to the centre of the manifold become smaller in comparison to the outer lines, thus approaching the true semiclassical spectrum, but that the asymmetry of the lines is exacerbated: They are clearly saw-tooth shaped, rising steeply on the left and falling off gently to the right.

At  $E \approx -4.7 \times 10^{-4}$ , neighbouring  $n$ -manifolds overlap for the first time, thus doubling the density of spectral lines. It can be seen in figure 8 that at this energy the harmonic inversion of the given semiclassical signal abruptly breaks down. It recovers at slightly higher energies, where again only levels of a single  $n$ -manifold are present. At  $E \approx -4.5 \times 10^{-4}$  and  $E \approx -4.2 \times 10^{-4}$ , pairs of levels belonging to different  $n$ -manifolds are so close to being degenerate that they cannot be resolved by the harmonic inversion. In the semiclassical spectrum they appear as single lines with amplitudes equal to the sum of the two quantum amplitudes.

Similar effects can also be observed at higher energies. However, as the energy and the density of spectral lines are further increased, the harmonic inversion gradually ceases to yield meaningful results. In the high-energy region at  $E \approx -3.2 \times 10^{-4}$ , a few lines can, somewhat arbitrarily, be identified, whereas most of the lines from the quantum spectrum are absent. In this region the cut-off time of the semiclassical signal is evidently, and expectedly, too small.

The harmonic inversion always yields some spurious spectral lines together with an error parameter  $\epsilon$  that can be used to distinguish between true and spurious lines [5]. In figure 8, only lines with an error parameter  $\epsilon < 6 \times 10^{-8}$  have been included. This threshold value will also be used for all other semiclassical spectra presented in this section. The selection of “good” semiclassical eigenvalues is therefore solely based on criteria inherent in the semiclassical quantization procedure, no lines are selected according to how well they fit the quantum results. As can be seen from figure 8, some spurious lines pass the selection. They are all characterized by having small amplitudes, so that they exert little influence on the semiclassical signal. Only rarely does it occur that a true spectral line of considerable amplitude is removed. If the region of overlapping  $n$ -manifolds, where the signal is too short to resolve the spectral lines, is ignored, the only instance of this error present in the above spectrum can be found at  $E \approx -5.1 \times 10^{-4}$ .

To improve the resolution, the cut-off time needs to be increased. As in the spectral region around  $E \approx -3.2 \times 10^{-4}$  three (or even four) different  $n$ -manifolds overlap, the true Heisenberg time can be expected to be close to three times its

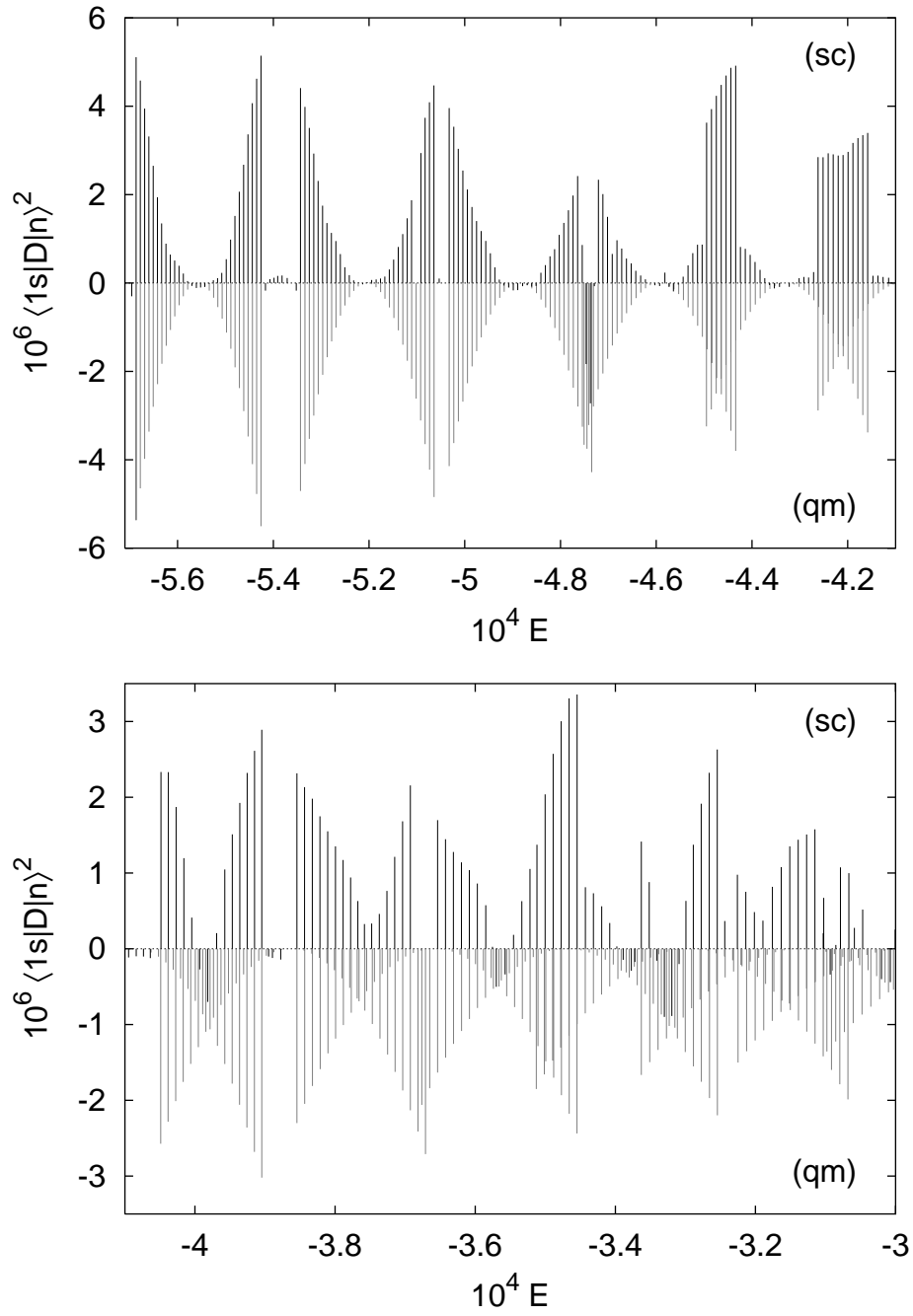


**Figure 8.** High-resolution semiclassical (sc) and quantum (qm, inverted) photo-absorption spectrum. The scaled cut-off time for the semiclassical spectrum is  $\tilde{T}_{\max} = 15$ .

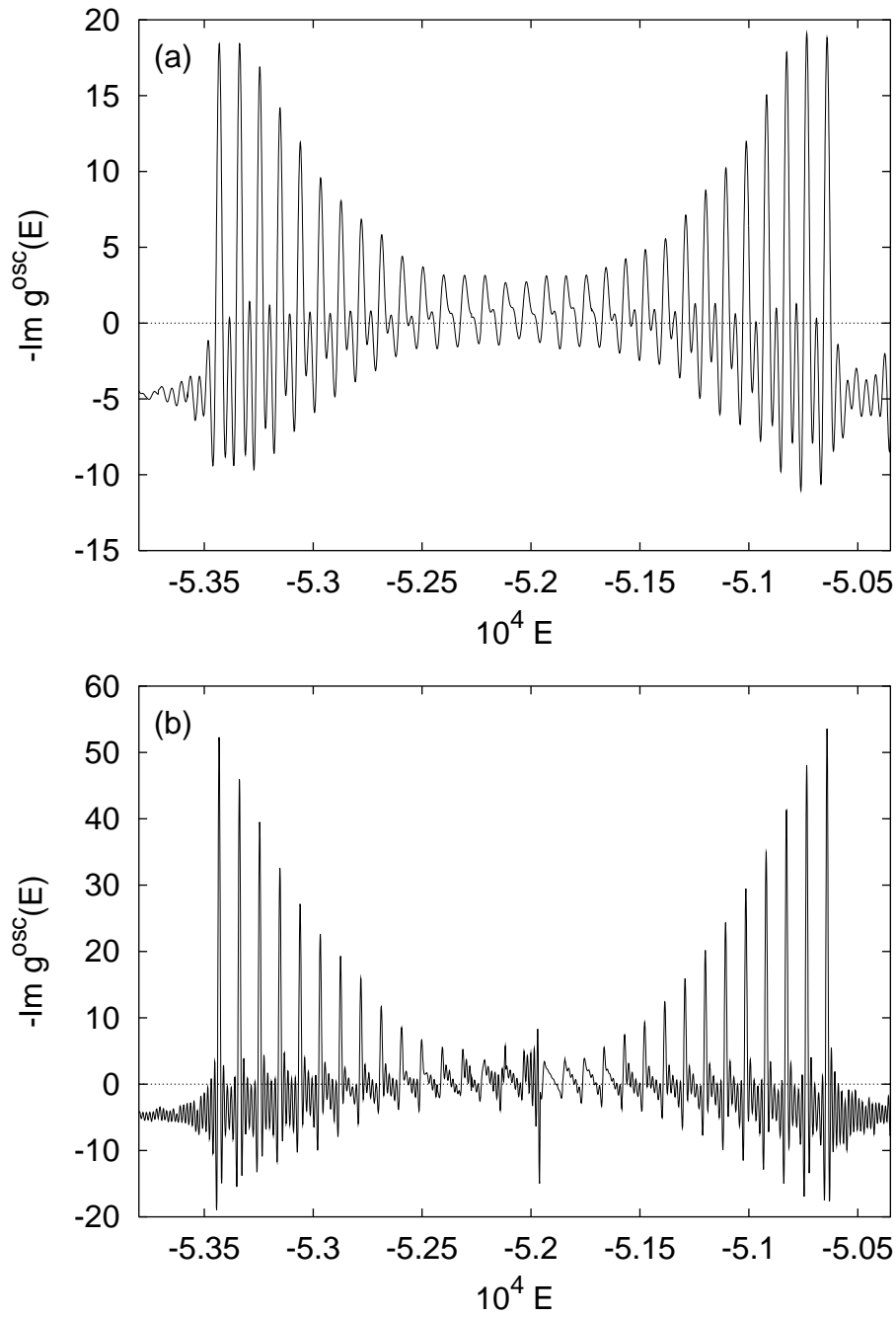


**Figure 9.** The manifold  $n = 31$  in the low-resolution semiclassical spectrum with scaled cut-off time (a)  $\tilde{T}_{\text{max}} = 15$  and (b)  $\tilde{T}_{\text{max}} = 40$ .

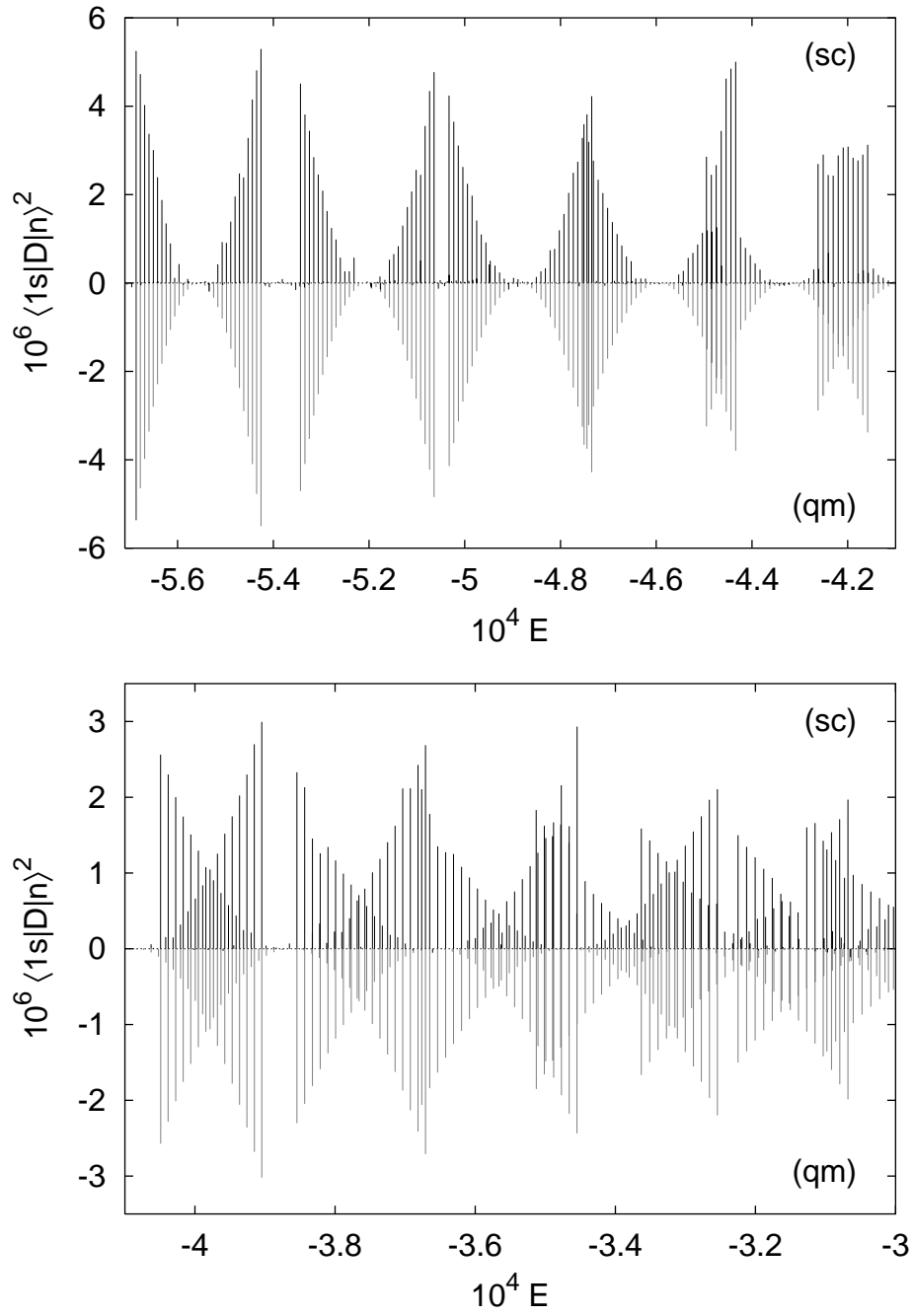


Figure 10. Same as figure 8 with  $\tilde{T}_{\max} = 40$ .

perturbative value. Figure 5 suggests choosing a scaled cut-off time of  $\tilde{T}_{\max} = 40$ . Results obtained with this semiclassical signal are shown in figure 10. In the low-energy spectral range, the amplitudes of the spurious lines have diminished. Thus, even in this range the longer signal yields a better semiclassical spectrum. In the region of overlapping  $n$ -manifolds around  $E \approx -3.8 \times 10^{-4}$ , all spectral lines are well resolved. At  $E \approx -3.2 \times 10^{-4}$ , groups of three closely spaced lines can be identified in the quantum spectrum. In many cases, all three of them are resolved in the semiclassical spectrum. In a few cases, nearly degenerate lines appear in the semiclassical spectrum as a single line whose amplitude is the sum of the two quantum amplitudes.

The most difficult spectral region appears at  $E \approx -4.2 \times 10^{-4}$ . In this region, spectral lines belonging to neighbouring  $n$ -manifold are so close to being degenerate that they are hard to distinguish even in the quantum spectrum. This degeneracy is somewhat accidental, as it will be lifted as the electric field strength is varied, but it nevertheless poses a particular challenge to the harmonic inversion. Even with the signal length of  $\tilde{T}_{\max} = 40$ , the degenerate levels cannot be resolved semiclassically. Their resolution would presumably require a significantly longer semiclassical signal. As an alternative, the harmonic inversion of cross-correlated signals has proven powerful in resolving nearly degenerate levels [20, 21]. It can be combined with the novel quantization procedure for non-scaling systems in an obvious way and can be expected to considerably reduce the signal length required to identify the unresolved spectral lines.

Results obtained with  $\tilde{T}_{\max} = 30$  for lower energies are shown in figure 11. In this region all  $n$ -manifolds are well isolated. As the splitting of levels within a manifold is smaller than at higher energies, the perturbative Heisenberg time is  $\tilde{T}_{\text{H,p}} = 9.4$  at  $E = -10^{-4}$ . Therefore, the chosen signal length should easily suffice to resolve the spectral lines. This is indeed achieved, the quantum and semiclassical spectra can be compared line by line. (Most of the small spurious lines between the manifolds can be removed if a stricter quality criterion for the semiclassical lines is applied. In figure 11, the same threshold  $\epsilon < 6 \times 10^{-8}$  as in previous figures is used.) However, the agreement between the spectra is not as perfect as was found at higher energies. In particular, considerable contributions to the semiclassical spectrum arise at the centres of the  $n$ -manifolds at low energies. This decrease in quality should be expected when the semiclassical approximation is applied to low-lying states. This is a fundamental limitation of semiclassical methods. In this case, however, a more subtle difficulty should be considered: Any non-axial orbit suffers two bifurcations, viz. its generations from the downhill orbit and its destruction at the uphill orbit. At low energies, the distance between the two bifurcations gets small, so that eventually they can no longer be regarded as isolated. At this point, the uniform approximation constructed in section 4 must fail. It must then be replaced with a uniform approximation describing both bifurcations collectively. Such an approximation can be constructed, but, contrary to all previous uniform approximations, it must use a spherical rather than Cartesian configuration space. This will be discussed in detail in a forthcoming publication [22].

An even harder uniformization problem arises close to the Stark saddle energy. As this energy is approached from below, the downhill orbits undergo an infinite sequence of bifurcations in a finite energy interval. Similar bifurcation cascades have been observed in the hydrogen atom in a magnetic field [23] and in Hénon-Heiles type systems [24]. Available techniques for the construction of uniform approximations can only take a finite number of bifurcating orbits into account, so that they do not allow



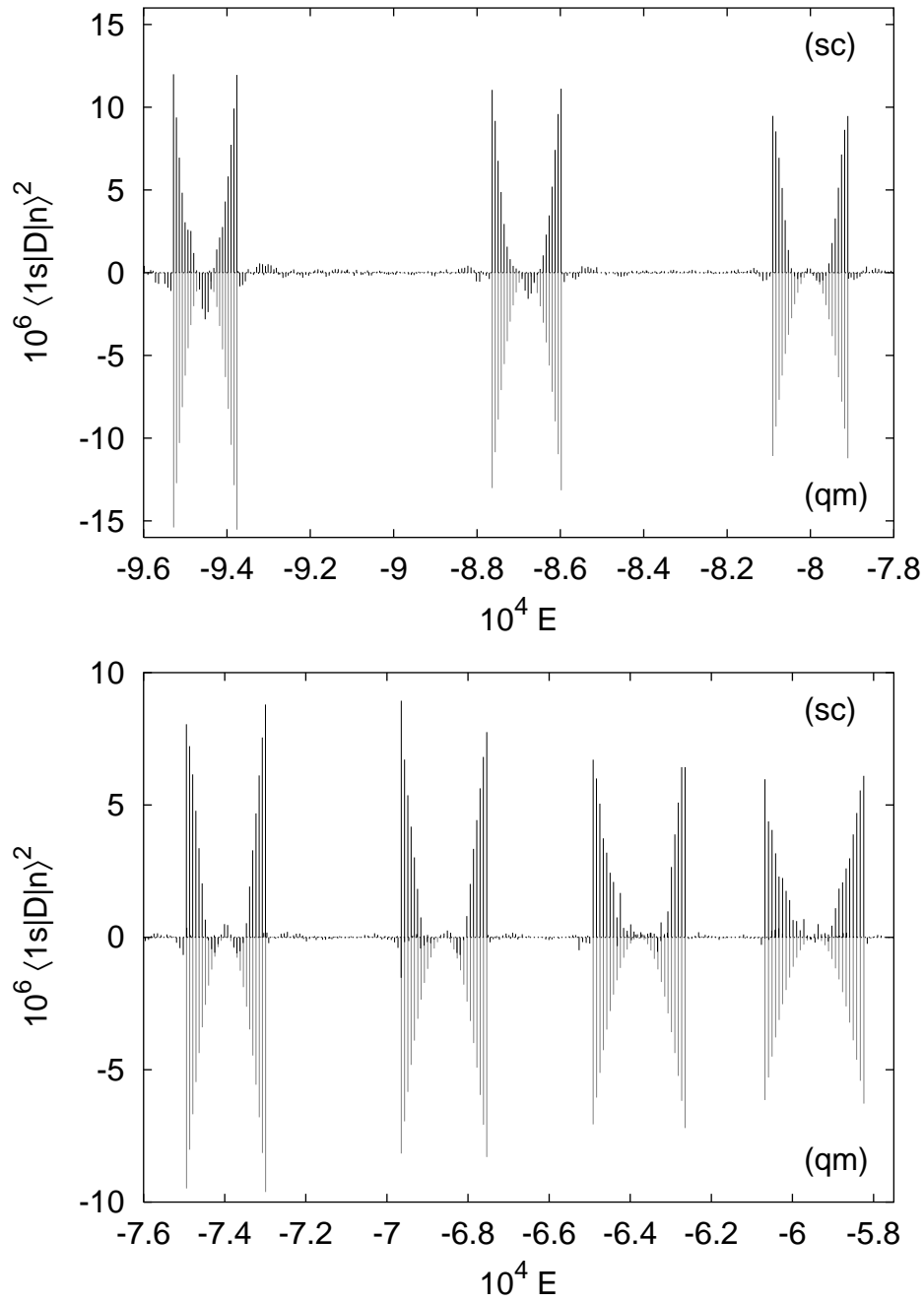


**Figure 11.** High-resolution semiclassical (sc) and quantum (qm, inverted) photo-absorption spectrum. The scaled cut-off time for the semiclassical spectrum is  $\tilde{T}_{\max} = 30$ .

the uniformization of an infinite cascade. For this reason, the spectral region around the Stark saddle energy was excluded from the calculations of the present paper.

## 6. Conclusion

In this paper we have solved the long standing problem of semiclassical quantization of the hydrogen atom in an electric field based on closed-orbit theory. We have presented a detailed study of both the classical dynamics of the hydrogen atom in an electric field and its semiclassical description in the framework of closed-orbit theory. The classical closed orbits were described, explicit formulae for the important orbital parameters were given, and the pattern of closed-orbit bifurcations was derived analytically. We constructed a particularly convenient form of the uniform semiclassical approximation for the closed-orbit bifurcations in the Stark system. Contrary to earlier versions, our uniform approximation can be computed from parameters characterizing the isolated orbits only, so that it is as easy to apply as the simple isolated-orbits approximation and can immediately be included into a closed-orbit summation.

We demonstrated that a semiclassical quantization of the hydrogen atom in an electric field by means of closed-orbit theory is impossible unless uniform approximations are included. By means of a generalized method of semiclassical quantization by harmonic inversion introduced recently [12], we were able to calculate high-quality semiclassical photo-absorption spectra from the uniformized closed-orbit sum. We thus proved that our novel method is indeed well suited to the extraction of high-resolution semiclassical spectra from low-resolution spectra of arbitrary systems, whether they are classically integrable, chaotic, or even mixed regular-chaotic. It thus paves the way to a semiclassical quantization of the hydrogen atom in a magnetic field or in crossed electric and magnetic fields. Further work on these more complicated, classically chaotic systems is in progress.

The present uniform approximation is applicable only as long as individual bifurcations can be regarded as isolated. It will fail if they are close. For this reason, the description of the spectral region close to the Stark saddle energy remains an open problem. At this energy, the downhill orbits undergo an infinite cascade of bifurcations in a finite energy interval. The uniformization of this kind of cascade is far beyond present-day techniques for the construction of uniform approximations. It presents a challenge worth-while for future research, both as a problem in its own right and in view of its potential applications: The bifurcation cascade occurs at the continuum threshold, where the transition from bound states to a continuum with embedded resonances takes place [2]. The semiclassical description of this transition region is a task of special importance. It will require the uniformization of the bifurcation cascades.

## References

- [1] Kondratovich V and Delos J B 1997 *Phys. Rev. A* **56** R5
- [2] Kondratovich V and Delos J B 1998 *Phys. Rev. A* **57** 4654
- [3] Du M L and Delos J B 1988 *Phys. Rev. A* **38** 1896 and 1913
- [4] Bogomolny E B 1989 *Sov. Phys. JETP* **69** 275
- [5] Bartsch T 2002 *The hydrogen atom in an electric field and in crossed electric and magnetic fields: Closed-orbit theory and semiclassical quantization*. (Göttingen, Germany: Cuvillier)
- [6] Bartsch T, Main J and Wunner G LANL preprint nlin.CD/0212017
- [7] Gutzwiller M C 1990 *Chaos in Classical and Quantum Mechanics* (New York: Springer-Verlag)

- [8] Gao J and Delos J B 1994 *Phys. Rev. A* **49** 869
- [9] Gao J and Delos J B 1997 *Phys. Rev. A* **56** 356
- [10] Shaw J A and Robicheaux F 1998 *Phys. Rev. A* **58** 1910
- [11] Shaw J A and Robicheaux F 1998 *Phys. Rev. A* **58** 3561
- [12] Bartsch T, Main J and Wunner G 2002 *Phys. Rev. A* **66** 033404
- [13] Born M 1925 *Vorlesungen über Atommechanik* (Berlin: Springer)
- [14] Landau L D and Lifshitz E M 1960 *Mechanics* (Oxford: Pergamon Press)
- [15] Dirac P A M 1933 *Proc. Camb. Phil. Soc.* **29** 389
- [16] Abramowitz M and Stegun I A 1984 *Pocketbook of Mathematical Functions* (Frankfurt/Main: Verlag Harri Deutsch)
- [17] Main J, Mandelshtam V A and Taylor H S 1997 *Phys. Rev. Lett.* **79** 825
- [18] Main J, Mandelshtam V A, Wunner G and Taylor H S 1998 *Nonlinearity* **11** 1015
- [19] Main J 1999 *Physics Reports* **316** 233
- [20] Main J, Weibert K, Mandelshtam V A and Wunner G 1999 *Phys. Rev. E* **60** 1639
- [21] Weibert K, Main J and Wunner G 2000 *Eur. Phys. J. D* **12** 381
- [22] Bartsch T, Main J and Wunner G To be published
- [23] Wintgen D 1987 *J. Phys. B* **20** L511
- [24] Brack M 2001 *Found. Phys.* **31** 209